

Measurement of branching fractions of singly Cabibbo-suppressed decays

$$\Lambda_c^+ \rightarrow \Sigma^0 K^+ \text{ and } \Sigma^+ K_S^0$$

M. Ablikim,¹ M. N. Achasov,^{11,b} P. Adlarson,⁷⁰ M. Albrecht,⁴ R. Aliberti,³¹ A. Amoroso,^{69a,69c} M. R. An,³⁵ Q. An,^{66,53} X. H. Bai,⁶¹ Y. Bai,⁵² O. Bakina,³² R. Baldini Ferroli,^{26a} I. Balossino,^{127a} Y. Ban,^{42,g} V. Batozskaya,^{1,40} D. Becker,³¹ K. Begzsuren,²⁹ N. Berger,³¹ M. Bertani,^{26a} D. Bettoni,^{27a} F. Bianchi,^{69a,69c} J. Bloms,⁶³ A. Bortone,^{69a,69c} I. Boyko,³² R. A. Briere,⁵ A. Brueggemann,⁶³ H. Cai,⁷¹ X. Cai,^{1,53} A. Calcaterra,^{26a} G. F. Cao,^{1,58} N. Cao,^{1,58} S. A. Cetin,^{57a} J. F. Chang,^{1,53} W. L. Chang,^{1,58} G. Chelkov,^{32,a} C. Chen,³⁹ Chao Chen,⁵⁰ G. Chen,¹ H. S. Chen,^{1,58} M. L. Chen,^{1,53} S. J. Chen,³⁸ S. M. Chen,⁵⁶ T. Chen,¹ X. R. Chen,^{28,58} X. T. Chen,¹ Y. B. Chen,^{1,53} Z. J. Chen,^{23,h} W. S. Cheng,^{69c} S. K. Choi,⁵⁰ X. Chu,³⁹ G. Cibinetto,^{27a} F. Cossio,^{69c} J. J. Cui,⁴⁵ H. L. Dai,^{1,53} J. P. Dai,⁷³ A. Dbeyssi,¹⁷ R. E. de Boer,⁴ D. Dedovich,³² Z. Y. Deng,¹ A. Denig,³¹ I. Denysenko,³² M. Destefanis,^{69a,69c} F. De Mori,^{69a,69c} Y. Ding,³⁶ J. Dong,^{1,53} L. Y. Dong,^{1,58} M. Y. Dong,^{1,53,58} X. Dong,⁷¹ S. X. Du,⁷⁵ P. Egorov,^{32,a} Y. L. Fan,⁷¹ J. Fang,^{1,53} S. S. Fang,^{1,58} W. X. Fang,¹ Y. Fang,¹ R. Farinelli,^{27a} L. Fava,^{69b,69c} F. Feldbauer,⁴ G. Felici,^{26a} C. Q. Feng,^{66,53} J. H. Feng,⁵⁴ K. Fischer,⁶⁴ M. Fritsch,⁴ C. Fritzscht,⁶³ C. D. Fu,¹ H. Gao,⁵⁸ Y. N. Gao,^{42,g} Yang Gao,^{66,53} S. Garbolino,^{69c} I. Garzia,^{27a,27b} P. T. Ge,⁷¹ Z. W. Ge,³⁸ C. Geng,⁵⁴ E. M. Gersabeck,⁶² A. Gilman,⁶⁴ K. Goetzen,¹² L. Gong,³⁶ W. X. Gong,^{1,53} W. Gradl,³¹ M. Greco,^{69a,69c} L. M. Gu,³⁸ M. H. Gu,^{1,53} Y. T. Gu,¹⁴ C. Y. Guan,^{1,58} A. Q. Guo,^{28,58} L. B. Guo,³⁷ R. P. Guo,⁴⁴ Y. P. Guo,^{10,f} A. Guskov,^{32,a} T. T. Han,⁴⁵ W. Y. Han,³⁵ X. Q. Hao,¹⁸ F. A. Harris,⁶⁰ K. K. He,⁵⁰ K. L. He,^{1,58} F. H. Heinsius,⁴ C. H. Heinz,³¹ Y. K. Heng,^{1,53,58} C. Herold,⁵⁵ M. Himmelreich,^{31,d} G. Y. Hou,^{1,58} Y. R. Hou,⁵⁸ Z. L. Hou,¹ H. M. Hu,^{1,58} J. F. Hu,^{51,i} T. Hu,^{1,53,58} Y. Hu,¹ G. S. Huang,^{66,53} K. X. Huang,⁵⁴ L. Q. Huang,⁶⁷ L. Q. Huang,^{28,58} X. T. Huang,⁴⁵ Y. P. Huang,¹ Z. Huang,^{42,g} T. Hussain,⁶⁸ N. Hüskens,^{25,31} W. Imoehl,²⁵ M. Irshad,^{66,53} J. Jackson,²⁵ S. Jaeger,⁴ S. Janchiv,²⁹ E. Jang,⁵⁰ J. H. Jeong,⁵⁰ Q. Ji,¹ Q. P. Ji,¹⁸ X. B. Ji,^{1,58} X. L. Ji,^{1,53} Y. Y. Ji,⁴⁵ Z. K. Jia,^{66,53} H. B. Jiang,⁴⁵ S. S. Jiang,³⁵ X. S. Jiang,^{1,53,58} Y. Jiang,⁵⁸ J. B. Jiao,⁴⁵ Z. Jiao,²¹ S. Jin,³⁸ Y. Jin,⁶¹ M. Q. Jing,^{1,58} T. Johansson,⁷⁰ N. Kalantar-Nayestanaki,⁵⁹ X. S. Kang,³⁶ R. Kappert,⁵⁹ M. Kavatsyuk,⁵⁹ B. C. Ke,⁷⁵ I. K. Keshk,⁴ A. Khoukaz,⁶³ P. Kiese,³¹ R. Kiuchi,¹ R. Kliemt,¹² L. Koch,³³ O. B. Kolcu,^{57a} B. Kopf,⁴ M. Kuemmel,⁴ M. Kuessner,⁴ A. Kupsc,^{40,70} W. Kühn,³³ J. J. Lane,⁶² J. S. Lange,³³ P. Larin,¹⁷ A. Lavania,²⁴ L. Lavezzi,^{69a,69c} Z. H. Lei,^{66,53} H. Leithoff,³¹ M. Lellmann,³¹ T. Lenz,³¹ C. Li,⁴³ C. Li,³⁹ C. H. Li,³⁵ Cheng Li,^{66,53} D. M. Li,⁷⁵ F. Li,^{1,53} G. Li,¹ H. Li,⁴⁷ H. Li,^{66,53} H. B. Li,^{1,58} H. J. Li,¹⁸ H. N. Li,^{51,i} J. Q. Li,⁴ J. S. Li,⁵⁴ J. W. Li,⁴⁵ Ke Li,¹ L. J. Li,¹ L. K. Li,¹ Lei Li,³ M. H. Li,³⁹ P. R. Li,^{34,j,k} S. X. Li,¹⁰ S. Y. Li,⁵⁶ T. Li,⁴⁵ W. D. Li,^{1,58} W. G. Li,¹ X. H. Li,^{66,53} X. L. Li,⁴⁵ Xiaoyu Li,^{1,58} H. Liang,^{66,53} H. Liang,^{1,58} H. Liang,³⁰ Y. F. Liang,⁴⁹ Y. T. Liang,^{28,58} G. R. Liao,¹³ L. Z. Liao,⁴⁵ J. Libby,²⁴ A. Limphirat,⁵⁵ C. X. Lin,⁵⁴ D. X. Lin,^{28,58} T. Lin,¹ B. J. Liu,¹ C. X. Liu,¹ D. Liu,^{17,66} F. H. Liu,⁴⁸ Fang Liu,¹ Feng Liu,⁶ G. M. Liu,^{51,i} H. Liu,^{34,j,k} H. B. Liu,¹⁴ H. M. Liu,^{1,58} Huanhuan Liu,¹ Huihui Liu,¹⁹ J. B. Liu,^{66,53} J. L. Liu,⁶⁷ J. Y. Liu,^{1,58} K. Liu,¹ K. Y. Liu,³⁶ Ke Liu,²⁰ L. Liu,^{66,53} Lu Liu,³⁹ M. H. Liu,^{10,f} P. L. Liu,¹ Q. Liu,⁵⁸ S. B. Liu,^{66,53} T. Liu,^{10,f} W. K. Liu,³⁹ W. M. Liu,^{66,53} X. Liu,^{34,j,k} Y. Liu,^{34,j,k} Y. B. Liu,³⁹ Z. A. Liu,^{1,53,58} Z. Q. Liu,⁴⁵ X. C. Lou,^{1,53,58} F. X. Lu,⁵⁴ H. J. Lu,²¹ J. G. Lu,^{1,53} X. L. Lu,¹ Y. Lu,⁷ Y. P. Lu,^{1,53} Z. H. Lu,¹ C. L. Luo,³⁷ M. X. Luo,⁷⁴ T. Luo,^{10,f} X. L. Luo,^{1,53} X. R. Lyu,⁵⁸ Y. F. Lyu,³⁹ F. C. Ma,³⁶ H. L. Ma,¹ L. L. Ma,⁴⁵ M. M. Ma,^{1,58} Q. M. Ma,¹ R. Q. Ma,^{1,58} R. T. Ma,⁵⁸ X. Y. Ma,^{1,53} Y. Ma,^{42,g} F. E. Maas,¹⁷ M. Maggiora,^{69a,69c} S. Maldaner,⁴ S. Malde,⁶⁴ Q. A. Malik,⁶⁸ A. Mangoni,^{26b} Y. J. Mao,^{42,g,g} Z. P. Mao,¹ S. Marcello,^{69a,69c} Z. X. Meng,⁶¹ J. G. Messchendorp,^{12,59} G. Mezzadri,^{127a} H. Miao,¹ T. J. Min,³⁸ R. E. Mitchell,²⁵ X. H. Mo,^{1,53,58} N. Yu. Muchnoi,^{11,b} Y. Nefedov,³² F. Nerling,^{17,d} I. B. Nikolaev,¹¹ Z. Ning,^{1,53} S. Nisar,^{9,l} Y. Niu,⁴⁵ S. L. Olsen,⁵⁸ Q. Ouyang,^{1,53,58} S. Pacetti,^{26b,26c} X. Pan,^{10,f} Y. Pan,⁵² A. Pathak,³⁰ M. Pelizaeus,⁴ H. P. Peng,^{66,53} K. Peters,^{12,d} J. Pettersson,⁷⁰ J. L. Ping,³⁷ R. G. Ping,^{1,58} S. Plura,³¹ S. Pogodin,³² V. Prasad,^{66,53} F. Z. Qi,¹ H. Qi,^{66,53} H. R. Qi,⁵⁶ M. Qi,³⁸ T. Y. Qi,^{10,f} S. Qian,^{1,53} W. B. Qian,⁵⁸ Z. Qian,⁵⁴ C. F. Qiao,⁵⁸ J. J. Qin,⁶⁷ L. Q. Qin,¹³ X. P. Qin,^{10,f} X. S. Qin,⁴⁵ Z. H. Qin,^{1,53} J. F. Qiu,¹ S. Q. Qu,³⁹ S. Q. Qu,⁵⁶ K. H. Rashid,⁶⁸ C. F. Redmer,³¹ K. J. Ren,³⁵ A. Rivetti,^{69c} V. Rodin,⁵⁹ M. Rolo,^{69c} G. Rong,^{1,58} Ch. Rosner,¹⁷ S. N. Ruan,³⁹ H. S. Sang,⁶⁶ A. Sarantsev,^{32,c} Y. Schelhaas,³¹ C. Schnier,⁴ K. Schönning,⁷⁰ M. Scodreggio,^{27a,27b} K. Y. Shan,^{10,f} W. Shan,²² X. Y. Shan,^{66,53} J. F. Shanguan,⁵⁰ L. G. Shao,^{1,58} M. Shao,^{66,53} C. P. Shen,^{10,f} H. F. Shen,^{1,58} X. Y. Shen,^{1,58} B. A. Shi,⁵⁸ H. C. Shi,^{66,53} J. Y. Shi,¹ q. q. Shi,⁵⁰ R. S. Shi,^{1,58} X. Shi,^{1,53} X. D. Shi,^{66,53} J. J. Song,¹⁸ W. M. Song,^{1,30} Y. X. Song,^{42,g} S. Sosio,^{69a,69c} S. Spataro,^{69a,69c} F. Stielert,³¹ K. X. Su,⁷¹ P. P. Su,⁵⁰ Y. J. Su,⁵⁸ G. X. Sun,¹ H. Sun,⁵⁸ H. K. Sun,¹ J. F. Sun,¹⁸ L. Sun,⁷¹ S. S. Sun,^{1,58} T. Sun,^{1,58} W. Y. Sun,³⁰ X. Sun,^{23,h} Y. J. Sun,^{66,53} Y. Z. Sun,¹ Z. T. Sun,⁴⁵ Y. H. Tan,⁷¹ Y. X. Tan,^{66,53} C. J. Tang,⁴⁹ G. Y. Tang,¹ J. Tang,⁵⁴ L. Y. Tao,⁶⁷ Q. T. Tao,^{23,h} M. Tat,⁶⁴ J. X. Teng,^{66,53} V. Thoren,⁷⁰ W. H. Tian,⁴⁷ Y. Tian,^{28,58} I. Uman,^{57b} B. Wang,¹ B. L. Wang,⁵⁸ C. W. Wang,³⁸ D. Y. Wang,^{42,g} F. Wang,⁶⁷ H. J. Wang,^{34,j,k} H. P. Wang,^{1,58} K. Wang,^{1,53} L. L. Wang,¹ M. Wang,⁴⁵ M. Z. Wang,^{42,g} Meng Wang,^{1,58} S. Wang,¹³ S. Wang,^{10,f} T. Wang,^{10,f} T. J. Wang,³⁹ W. Wang,⁵⁴ W. H. Wang,⁷¹ W. P. Wang,^{66,53} X. Wang,^{42,g} X. F. Wang,^{34,j,k} X. L. Wang,^{10,f} Y. D. Wang,⁴¹ Y. F. Wang,^{1,53,58} Y. H. Wang,⁴³ Y. Q. Wang,¹ Yaqian Wang,^{1,16} Yi Wang,⁵⁶ Z. Wang,^{1,53} Z. Y. Wang,^{1,58} Ziyi Wang,⁵⁸ D. H. Wei,¹³ F. Weidner,⁶³ S. P. Wen,¹ D. J. White,⁶² U. Wiedner,⁴ G. Wilkinson,⁶⁴ M. Wolke,⁷⁰ L. Wollenberg,⁴ J. F. Wu,^{1,58} L. H. Wu,¹

L. J. Wu,^{1,58} X. Wu,^{10,f} X. H. Wu,³⁰ Y. Wu,⁶⁶ Z. Wu,^{1,53} L. Xia,^{66,53} T. Xiang,^{42,g} D. Xiao,^{34,j,k} G. Y. Xiao,³⁸ H. Xiao,^{10,f}
 S. Y. Xiao,¹ Y. L. Xiao,^{10,f} Z. J. Xiao,³⁷ C. Xie,³⁸ X. H. Xie,^{42,g} Y. Xie,⁴⁵ Y. G. Xie,^{1,53} Y. H. Xie,⁶ Z. P. Xie,^{66,53}
 T. Y. Xing,^{1,58} C. F. Xu,¹ C. J. Xu,⁵⁴ G. F. Xu,¹ H. Y. Xu,⁶¹ Q. J. Xu,¹⁵ S. Y. Xu,⁶⁵ X. P. Xu,⁵⁰ Y. C. Xu,⁵⁸ Z. P. Xu,³⁸ F. Yan,^{10,}
^f L. Yan,^{10,f} W. B. Yan,^{66,53} W. C. Yan,⁷⁵ H. J. Yang,^{46,e} H. L. Yang,³⁰ H. X. Yang,¹ L. Yang,⁴⁷ S. L. Yang,⁵⁸ Tao Yang,¹
 Y. F. Yang,³⁹ Y. X. Yang,^{1,58} Yifan Yang,^{1,58} M. Ye,^{1,53} M. H. Ye,⁸ J. H. Yin,¹ Z. Y. You,⁵⁴ B. X. Yu,^{1,53,58} C. X. Yu,³⁹
 G. Yu,^{1,58} T. Yu,⁶⁷ X. D. Yu,^{42,g} C. Z. Yuan,^{1,58} L. Yuan,² S. C. Yuan,¹ X. Q. Yuan,¹ Y. Yuan,^{1,58} Z. Y. Yuan,⁵⁴ C. X. Yue,³⁵
 A. A. Zafar,⁶⁸ F. R. Zeng,⁴⁵ X. Zeng,⁶ Y. Zeng,^{23,h} Y. H. Zhan,⁵⁴ A. Q. Zhang,¹ B. L. Zhang,¹ B. X. Zhang,¹ D. H. Zhang,³⁹
 G. Y. Zhang,¹⁸ H. Zhang,⁶⁶ H. H. Zhang,⁵⁴ H. H. Zhang,³⁰ H. Y. Zhang,^{1,53} J. L. Zhang,⁷² J. Q. Zhang,³⁷ J. W. Zhang,^{1,53,58}
 J. X. Zhang,^{34,j,k} J. Y. Zhang,¹ J. Z. Zhang,^{1,58} Jianyu Zhang,^{1,58} Jiawei Zhang,^{1,58} L. M. Zhang,⁵⁶ L. Q. Zhang,⁵⁴
 Lei Zhang,³⁸ P. Zhang,¹ Q. Y. Zhang,^{35,75} Shulei Zhang,^{23,h} X. D. Zhang,⁴¹ X. M. Zhang,¹ X. Y. Zhang,⁴⁵ X. Y. Zhang,⁵⁰
 Y. Zhang,⁶⁴ Y. T. Zhang,⁷⁵ Y. H. Zhang,^{1,53} Yan Zhang,^{66,53} Yao Zhang,¹ Z. H. Zhang,¹ Z. Y. Zhang,⁷¹ Z. Y. Zhang,³⁹
 G. Zhao,¹ J. Zhao,³⁵ J. Y. Zhao,^{1,58} J. Z. Zhao,^{1,53} Lei Zhao,^{66,53} Ling Zhao,¹ M. G. Zhao,³⁹ Q. Zhao,¹ S. J. Zhao,⁷⁵
 Y. B. Zhao,^{1,53} Y. X. Zhao,^{28,58} Z. G. Zhao,^{66,53} A. Zhemchugov,^{32,a} B. Zheng,⁶⁷ J. P. Zheng,^{1,53} Y. H. Zheng,⁵⁸ B. Zhong,³⁷
 C. Zhong,⁶⁷ X. Zhong,⁵⁴ H. Zhou,⁴⁵ L. P. Zhou,^{1,58} X. Zhou,⁷¹ X. K. Zhou,⁵⁸ X. R. Zhou,^{66,53} X. Y. Zhou,³⁵ Y. Z. Zhou,^{10,f}
 J. Zhu,³⁹ K. Zhu,¹ K. J. Zhu,^{1,53,58} L. X. Zhu,⁵⁸ S. H. Zhu,⁶⁵ S. Q. Zhu,³⁸ T. J. Zhu,⁷² W. J. Zhu,^{10,f} Y. C. Zhu,^{66,53}
 Z. A. Zhu,^{1,58} B. S. Zou,¹ and J. H. Zou¹

(BESIII Collaboration)

¹*Institute of High Energy Physics, Beijing 100049, People's Republic of China*

²*Beihang University, Beijing 100191, People's Republic of China*

³*Beijing Institute of Petrochemical Technology, Beijing 102617, People's Republic of China*

⁴*Bochum Ruhr-University, D-44780 Bochum, Germany*

⁵*Carnegie Mellon University, Pittsburgh, Pennsylvania 15213, USA*

⁶*Central China Normal University, Wuhan 430079, People's Republic of China*

⁷*Central South University, Changsha 410083, People's Republic of China*

⁸*China Center of Advanced Science and Technology, Beijing 100190, People's Republic of China*

⁹*COMSATS University Islamabad, Lahore Campus, Defence Road,
Off Raiwind Road, 54000 Lahore, Pakistan*

¹⁰*Fudan University, Shanghai 200433, People's Republic of China*

¹¹*G.I. Budker Institute of Nuclear Physics SB RAS (BINP), Novosibirsk 630090, Russia*

¹²*GSI Helmholtzcentre for Heavy Ion Research GmbH, D-64291 Darmstadt, Germany*

¹³*Guangxi Normal University, Guilin 541004, People's Republic of China*

¹⁴*Guangxi University, Nanning 530004, People's Republic of China*

¹⁵*Hangzhou Normal University, Hangzhou 310036, People's Republic of China*

¹⁶*Hebei University, Baoding 071002, People's Republic of China*

¹⁷*Helmholtz Institute Mainz, Staudinger Weg 18, D-55099 Mainz, Germany*

¹⁸*Henan Normal University, Xinxiang 453007, People's Republic of China*

¹⁹*Henan University of Science and Technology, Luoyang 471003, People's Republic of China*

²⁰*Henan University of Technology, Zhengzhou 450001, People's Republic of China*

²¹*Huangshan College, Huangshan 245000, People's Republic of China*

²²*Hunan Normal University, Changsha 410081, People's Republic of China*

²³*Hunan University, Changsha 410082, People's Republic of China*

²⁴*Indian Institute of Technology Madras, Chennai 600036, India*

²⁵*Indiana University, Bloomington, Indiana 47405, USA*

^{26a}*INFN Laboratori Nazionali di Frascati, I-00044, Frascati, Italy*

^{26b}*INFN Sezione di Perugia, I-06100, Perugia, Italy*

^{26c}*University of Perugia, I-06100, Perugia, Italy*

^{27a}*INFN Sezione di Ferrara, I-44122, Ferrara, Italy*

^{27b}*University of Ferrara, I-44122, Ferrara, Italy*

²⁸*Institute of Modern Physics, Lanzhou 730000, People's Republic of China*

²⁹*Institute of Physics and Technology, Peace Avenue 54B, Ulaanbaatar 13330, Mongolia*

³⁰*Jilin University, Changchun 130012, People's Republic of China*

³¹*Johannes Gutenberg University of Mainz, Johann-Joachim-Becher-Weg 45, D-55099 Mainz, Germany*

³²*Joint Institute for Nuclear Research, 141980 Dubna, Moscow region, Russia*

³³*Justus-Liebig-Universitaet Giessen, II. Physikalisches Institut, Heinrich-Buff-Ring 16,
D-35392 Giessen, Germany*

³⁴*Lanzhou University, Lanzhou 730000, People's Republic of China*

³⁵*Liaoning Normal University, Dalian 116029, People's Republic of China*

³⁶*Liaoning University, Shenyang 110036, People's Republic of China*

- ³⁷Nanjing Normal University, Nanjing 210023, People's Republic of China
³⁸Nanjing University, Nanjing 210093, People's Republic of China
³⁹Nankai University, Tianjin 300071, People's Republic of China
⁴⁰National Centre for Nuclear Research, Warsaw 02-093, Poland
⁴¹North China Electric Power University, Beijing 102206, People's Republic of China
⁴²Peking University, Beijing 100871, People's Republic of China
⁴³Qufu Normal University, Qufu 273165, People's Republic of China
⁴⁴Shandong Normal University, Jinan 250014, People's Republic of China
⁴⁵Shandong University, Jinan 250100, People's Republic of China
⁴⁶Shanghai Jiao Tong University, Shanghai 200240, People's Republic of China
⁴⁷Shanxi Normal University, Linfen 041004, People's Republic of China
⁴⁸Shanxi University, Taiyuan 030006, People's Republic of China
⁴⁹Sichuan University, Chengdu 610064, People's Republic of China
⁵⁰Soochow University, Suzhou 215006, People's Republic of China
⁵¹South China Normal University, Guangzhou 510006, People's Republic of China
⁵²Southeast University, Nanjing 211100, People's Republic of China
⁵³State Key Laboratory of Particle Detection and Electronics, Beijing 100049, Hefei 230026, People's Republic of China
⁵⁴Sun Yat-Sen University, Guangzhou 510275, People's Republic of China
⁵⁵Suranaree University of Technology, University Avenue 111, Nakhon Ratchasima 30000, Thailand
⁵⁶Tsinghua University, Beijing 100084, People's Republic of China
^{57a}Turkish Accelerator Center Particle Factory Group, Istinye University, 34010, Istanbul, Turkey
^{57b}Near East University, Nicosia, North Cyprus, Mersin 10, Turkey
⁵⁸University of Chinese Academy of Sciences, Beijing 100049, People's Republic of China
⁵⁹University of Groningen, NL-9747 AA Groningen, Netherlands
⁶⁰University of Hawaii, Honolulu, Hawaii 96822, USA
⁶¹University of Jinan, Jinan 250022, People's Republic of China
⁶²University of Manchester, Oxford Road, Manchester, M13 9PL, United Kingdom
⁶³University of Muenster, Wilhelm-Klemm-Strasse 9, 48149 Muenster, Germany
⁶⁴University of Oxford, Keble Road, Oxford, United Kingdom OX13RH
⁶⁵University of Science and Technology Liaoning, Anshan 114051, People's Republic of China
⁶⁶University of Science and Technology of China, Hefei 230026, People's Republic of China
⁶⁷University of South China, Hengyang 421001, People's Republic of China
⁶⁸University of the Punjab, Lahore-54590, Pakistan
^{69a}University of Turin and INFN, University of Turin, I-10125, Turin, Italy
^{69b}University of Eastern Piedmont, I-15121, Alessandria, Italy
^{69c}INFN, I-10125, Turin, Italy
⁷⁰Uppsala University, Box 516, SE-75120 Uppsala, Sweden
⁷¹Wuhan University, Wuhan 430072, People's Republic of China
⁷²Xinyang Normal University, Xinyang 464000, People's Republic of China
⁷³Yunnan University, Kunming 650500, People's Republic of China
⁷⁴Zhejiang University, Hangzhou 310027, People's Republic of China
⁷⁵Zhengzhou University, Zhengzhou 450001, People's Republic of China

^aAlso at the Moscow Institute of Physics and Technology, Moscow 141700, Russia.

^bAlso at the Novosibirsk State University, Novosibirsk, 630090, Russia.

^cAlso at the NRC "Kurchatov Institute", PNPI, 188300, Gatchina, Russia.

^dAlso at Goethe University Frankfurt, 60323 Frankfurt am Main, Germany.

^eAlso at Key Laboratory for Particle Physics, Astrophysics and Cosmology, Ministry of Education; Shanghai Key Laboratory for Particle Physics and Cosmology; Institute of Nuclear and Particle Physics, Shanghai 200240, People's Republic of China.

^fAlso at Key Laboratory of Nuclear Physics and Ion-beam Application (MOE) and Institute of Modern Physics, Fudan University, Shanghai 200443, People's Republic of China.

^gAlso at State Key Laboratory of Nuclear Physics and Technology, Peking University, Beijing 100871, People's Republic of China.

^hAlso at School of Physics and Electronics, Hunan University, Changsha 410082, China.

ⁱAlso at Guangdong Provincial Key Laboratory of Nuclear Science, Institute of Quantum Matter, South China Normal University, Guangzhou 510006, China.

^jAlso at Frontiers Science Center for Rare Isotopes, Lanzhou University, Lanzhou 730000, People's Republic of China.

^kAlso at Lanzhou Center for Theoretical Physics, Lanzhou University, Lanzhou 730000, People's Republic of China.

^lAlso at the Department of Mathematical Sciences, IBA, Karachi, Pakistan.

 (Received 25 July 2022; accepted 8 August 2022; published 8 September 2022)

Based on a sample of 4.5 fb^{-1} of e^+e^- annihilation data collected in the energy region between 4.6 GeV and 4.7 GeV with the BESIII detector at BEPCII, two singly Cabibbo-suppressed decays $\Lambda_c^+ \rightarrow \Sigma^0 K^+$ and $\Lambda_c^+ \rightarrow \Sigma^+ K_S^0$ are studied. The ratio of the branching fraction $\mathcal{B}(\Lambda_c^+ \rightarrow \Sigma^0 K^+)$ relative to $\mathcal{B}(\Lambda_c^+ \rightarrow \Sigma^0 \pi^+)$ is measured to be $0.0361 \pm 0.0073(\text{stat.}) \pm 0.0005(\text{syst.})$, and the ratio of $\mathcal{B}(\Lambda_c^+ \rightarrow \Sigma^+ K_S^0)$ relative to $\mathcal{B}(\Lambda_c^+ \rightarrow \Sigma^+ \pi^+ \pi^-)$ is measured to be $0.0106 \pm 0.0031(\text{stat.}) \pm 0.0004(\text{syst.})$. After taking the world-average branching fractions of the reference decay channels, the branching fractions $\mathcal{B}(\Lambda_c^+ \rightarrow \Sigma^0 K^+)$ and $\mathcal{B}(\Lambda_c^+ \rightarrow \Sigma^+ K_S^0)$ are determined to be $(4.7 \pm 0.9(\text{stat.}) \pm 0.1(\text{syst.}) \pm 0.3(\text{ref.})) \times 10^{-4}$ and $(4.8 \pm 1.4(\text{stat.}) \pm 0.2(\text{syst.}) \pm 0.3(\text{ref.})) \times 10^{-4}$, respectively. The branching fraction of the $\Lambda_c^+ \rightarrow \Sigma^+ K_S^0$ decay is measured for the first time.

DOI: [10.1103/PhysRevD.106.052003](https://doi.org/10.1103/PhysRevD.106.052003)

I. INTRODUCTION

The study of charmed baryon decays is valuable for both understanding charmed-baryon dynamics and probing the effects of the weak and strong interactions. Since the ground state of the charmed baryons Λ_c^+ was discovered [1], many efforts have been made to predict its branching fractions (BFs) into two-body hadronic final states, $\Lambda_c^+ \rightarrow B_n M$ [2–7], where B_n and M denote the octet baryon and nonet meson states, respectively. However, progress has been hindered, due to the limited precision of experimental measurements [8] and difficulties in the theoretical treatment of nonperturbative strong interaction effects. For example, before studies of singly Cabibbo-suppressed (SCS) Λ_c^+ decays were performed by the Belle [9] and BABAR [10] collaborations, only one theoretical calculation existed for the BFs of these SCS processes [2]. Throughout this paper, the charge-conjugate modes are implied, unless otherwise stated.

The challenge for theoretical predictions is that the well-known factorization approach, which has been applied successfully to heavy-meson decays, has difficulties in describing charmed-baryon decays [11]. This is because the nonfactorizable terms are sizable or even dominant contributions in Λ_c^+ hadronic decays [2], compared with the charmed-meson case [12,13], e.g., the SCS $\Lambda_c^+ \rightarrow \Sigma^0 K^+$ and $\Sigma^+ K_S^0$ decays *only* receive nonfactorizable contribution. These nonfactorizable terms, arising from W -exchange or internal W -emission [3], can be constrained by precise experimental inputs in charmed-meson decays [14].

The BESIII collaboration [15] has reported significant improvements in the precision of absolute hadronic BFs of the Λ_c baryon, and the first model-independent

measurements near the threshold of $\Lambda_c^+ \bar{\Lambda}_c^-$ production [16]. In addition, the BESIII, LHCb and Belle collaborations have carried out complementary analyses of charmed baryons, such as lifetime measurements [17–21] and studies of semileptonic decays [22–26]. Improved measurements of the BFs of the Λ_c decays can provide crucial inputs for the theoretical models [3–6], in particular those of the SCS $\Lambda_c \rightarrow \Sigma K$ decays for which there exists very limited experimental information.

Theoretical predictions for SCS Λ_c decays are listed in Table I. In Refs. [2,3], factorizable terms are made accessible by inserting vacuum intermediates states [2], which are then reduced to the products of current matrix elements defined with decay constants of the emitted meson M and form factors of the $\Lambda_c^+ \rightarrow B_n$ transition. Nonfactorizable terms are tackled in the current algebra framework with the pole approximation in Refs. [2,3]. Reference [3] uses the MIT bag model [27] to account for baryon pole transition matrix elements, while Ref. [2] makes short-distance QCD corrections to the weak Hamiltonian. In Ref. [4], a diagrammatic analysis is performed and $\mathcal{B}(\Lambda_c^+ \rightarrow \Sigma^+ K_S^0)$ is predicted to be $(9.6 \pm 2.4) \times 10^{-4}$. Reference [5] expects that $\mathcal{B}(\Lambda_c^+ \rightarrow \Sigma^0 K^+) = \mathcal{B}(\Lambda_c^+ \rightarrow \Sigma^+ K_S^0) = (5.4 \pm 0.7) \times 10^{-4}$ under $SU(3)_F$ flavor symmetry. In Ref. [6], the irreducible representation amplitude (IRA) approach is used to extract amplitudes from experimental data inputs, which gives quite different predictions for $\mathcal{B}(\Lambda_c^+ \rightarrow \Sigma^0 K^+)$ and $\mathcal{B}(\Lambda_c^+ \rightarrow \Sigma^+ K_S^0)$. In particular, Ref. [6] predicts that $\mathcal{B}(\Lambda_c^+ \rightarrow \Sigma^+ K_S^0)$ is about one fifth of $\mathcal{B}(\Lambda_c^+ \rightarrow \Sigma^0 K^+)$, which is far smaller than other predictions.

Table I shows the current Particle Data Group (PDG) [28] world average value of $\mathcal{B}(\Lambda_c^+ \rightarrow \Sigma^0 K^+)$ based on measurements from the Belle [9] and BABAR [10] collaborations, performed more than a decade ago, while no measurement exists for the $\Lambda_c^+ \rightarrow \Sigma^+ K_S^0$ decay. All theoretical predictions for $\mathcal{B}(\Lambda_c^+ \rightarrow \Sigma^0 K^+)$ are consistent with the experimental value. Those predictions in Refs. [4–6] are from fits that take an ensemble of measured BFs as inputs, and are limited by the precision of these

Published by the American Physical Society under the terms of the [Creative Commons Attribution 4.0 International license](https://creativecommons.org/licenses/by/4.0/). Further distribution of this work must maintain attribution to the author(s) and the published article's title, journal citation, and DOI. Funded by SCOAP³.

TABLE I. Comparison of various theoretical predictions and the experimental values for $\mathcal{B}(\Lambda_c^+ \rightarrow \Sigma K)$ (in unit of 10^{-4}). In Ref. [2], alternative assignments to QCD corrections give different predictions as shown in the parentheses. The theoretical uncertainties in Ref. [3] are estimated to be 25%, arising from a slight change of the MIT bag radius.

| | $\mathcal{B}(\Lambda_c^+ \rightarrow \Sigma^0 K^+)$ | $\mathcal{B}(\Lambda_c^+ \rightarrow \Sigma^+ K_S^0)$ |
|-------------------------------|---|---|
| QCD corrections [2] | 2(8) | 2(4) |
| MIT bag model [3] | 7.2 ± 1.8 | 7.2 ± 1.8 |
| Diagrammatic analysis [4] | 5.5 ± 1.6 | 9.6 ± 2.4 |
| $SU(3)_F$ flavor symmetry [5] | 5.4 ± 0.7 | 5.4 ± 0.7 |
| IRA method [6] | 5.0 ± 0.6 | 1.0 ± 0.4 |
| PDG 2020 [28] | 5.2 ± 0.8 | ... |

measurements. Thus, new determinations of the BFs of $\Lambda_c \rightarrow \Sigma K$ decays, in particular the mode $\Lambda_c^+ \rightarrow \Sigma^+ K_S^0$, are important for validating and improving these theoretical-model calculations. Furthermore, improved measurements may clarify the tension between the predictions in Ref. [6] and Refs. [2–5].

In this paper, we present a study of the SCS decays $\Lambda_c^+ \rightarrow \Sigma^0 K^+$ and $\Sigma^+ K_S^0$ based on 4.5 fb^{-1} of e^+e^- annihilation data collected at the center-of-mass energies $\sqrt{s} = 4.600, 4.612, 4.628, 4.641, 4.661, 4.682, 4.699 \text{ GeV}$ [29,30] with the BESIII detector at BEPCII. We report the first study of the channel $\Lambda_c^+ \rightarrow \Sigma^+ K_S^0$ and provide the BF ratio, $\mathcal{B}(\Lambda_c^+ \rightarrow \Sigma^+ K_S^0)/\mathcal{B}(\Lambda_c^+ \rightarrow \Sigma^+ \pi^+ \pi^-)$, together with an improved measurement of the BF ratio, $\mathcal{B}(\Lambda_c^+ \rightarrow \Sigma^0 K^+)/\mathcal{B}(\Lambda_c^+ \rightarrow \Sigma^0 \pi^+)$.

II. BESIII EXPERIMENT AND MONTE CARLO SIMULATION

The BESIII detector [31] records symmetric e^+e^- collisions provided by the BEPCII storage ring [32] in the center-of-mass energy range from 2.0 to 4.95 GeV, with a peak luminosity of $1 \times 10^{33} \text{ cm}^{-2} \text{ s}^{-1}$ achieved at $\sqrt{s} = 3.77 \text{ GeV}$. The cylindrical core of the BESIII detector covers 93% of the full solid angle and consists of a helium-based multilayer drift chamber (MDC), a plastic scintillator time-of-flight system (TOF), and a CsI(Tl) electromagnetic calorimeter (EMC), which are all enclosed in a superconducting solenoidal magnet providing a 1.0 T magnetic field. The solenoid is supported by an octagonal flux-return yoke with resistive plate counter muon identification modules interleaved with steel. The charged-particle momentum resolution at 1 GeV/c is 0.5%, and the ionization energy loss dE/dx resolution is 6% for electrons from Bhabha scattering. The EMC measures photon energies with a resolution of 2.5% (5%) at 1 GeV in the barrel (end-cap) region. The time resolution in the TOF barrel region is 68 ps, while that in the end-cap region is 110 ps. The endcap TOF system was upgraded in 2015 using multigap resistive plate chamber technology,

providing a time resolution of 60 ps [33]. More detailed descriptions can be found in Refs. [31,32].

Simulated data samples are produced with a GEANT4-based [34] Monte Carlo (MC) package, which includes the geometric description of the BESIII detector [35,36] and the detector response. The simulation models the beam-energy spread and initial-state radiation (ISR) in the e^+e^- annihilations with the generator KKMC [37]. The final-state radiation from charged final-state particles is incorporated using PHOTOS [38].

The ‘‘inclusive MC sample’’ includes the production of $\Lambda_c^+ \bar{\Lambda}_c^-$ pairs and open-charmed mesons, ISR production of vector charmonium(-like) states, and continuum processes which are incorporated in KKMC [37,39]. Known decay modes are modeled with EVTGEN [40,41] using the BFs taken from the PDG [28]. The BF $\mathcal{B}(\Lambda_c^+ \rightarrow \Sigma^+ K_S^0)$ is assumed to be the same as $\mathcal{B}(\Lambda_c^+ \rightarrow \Sigma^0 K^+)$. The remaining unknown charmonium decays are modeled with LUNDCHARM [42,43]. The inclusive MC sample is used to study background contributions and to optimize event selections. We denote ‘‘Hadron MC’’ as the inclusive MC sample with $\Lambda_c^+ \bar{\Lambda}_c^-$ pairs removed, which therefore only includes backgrounds for this study. For the reference mode $\Lambda_c^+ \rightarrow \Sigma^+ \pi^+ \pi^-$, the intermediate states are modeled according to an internal partial-wave analysis of this channel. For the reference mode $\Lambda_c^+ \rightarrow \Sigma^0 \pi^+$, the angular distributions are described with consideration of the transverse polarization and decay asymmetry parameters of the Λ_c^+ and its daughter baryons [44]. Due to current limited statistics of data, the decay asymmetry parameters of the signal SCS decays $\Lambda_c^+ \rightarrow \Sigma^0 K^+$ and $\Sigma^+ K_S^0$ are not well determined. Thus, we use a uniformly distributed phase-space model for the simulation of the signal SCS decays. We then evaluate the systematic uncertainties of the unknown decay asymmetry parameters in Sec. V. The $e^+e^- \rightarrow \Lambda_c^+ \bar{\Lambda}_c^-$ ‘‘signal MC’’ samples, in which the Λ_c^+ decays exclusively into signal (reference) modes while the $\bar{\Lambda}_c^-$ decays inclusively, are used to determine the detection efficiencies.

III. EVENT SELECTION

In this analysis, we reconstruct the two signal modes through the cascade decays $\Lambda_c^+ \rightarrow \Sigma^0 K^+, \Sigma^0 \rightarrow \gamma \Lambda, \Lambda \rightarrow p \pi^-$ and $\Lambda_c^+ \rightarrow \Sigma^+ K_S^0, \Sigma^+ \rightarrow p \pi^0, \pi^0 \rightarrow \gamma \gamma, K_S^0 \rightarrow \pi^+ \pi^-$. The reference modes $\Lambda_c^+ \rightarrow \Sigma^0 \pi^+$ and $\Sigma^+ \pi^+ \pi^-$ are reconstructed through the same decay chains of the Σ^0 and Σ^+ baryons. As the $\Lambda_c^+ \bar{\Lambda}_c^-$ pair is produced without any accompanying hadrons, it is possible to reconstruct the Λ_c^+ and infer the presence of the $\bar{\Lambda}_c^-$ through its recoil mass.

Charged tracks are reconstructed in the MDC, and are required to have a polar angle θ with respect to the z -axis, defined as the symmetry axis of the MDC, satisfying $|\cos \theta| < 0.93$. Those tracks that are not used in the

reconstruction of $K_S^0 \rightarrow \pi^+\pi^-$ and $\Lambda \rightarrow p\pi^-$ candidates must have a distance of closest approach to the interaction point (IP) smaller than 10 cm along the z -axis (V_z) and smaller than 1 cm in the perpendicular plane (V_r). Particle identification (PID) for charged tracks is implemented [45] using combined information from the flight time measured in the TOF and the dE/dx measured in the MDC. Charged tracks are identified as protons when they satisfy $\mathcal{L}(p) > \mathcal{L}(K)$, $\mathcal{L}(p) > \mathcal{L}(\pi)$ and $\mathcal{L}(p) > 0.0001$, where $\mathcal{L}(h)$ is the PID probability for each hadron (h) hypothesis with $h = p, \pi, K$. Charged tracks are identified as pions when they satisfy $\mathcal{L}(\pi) > \mathcal{L}(K)$. In the selection of $\Lambda_c^+ \rightarrow \Sigma^0 K^+$ and $\Sigma^0 \pi^+$ decays, no PID requirement is imposed for the bachelor kaons and pions, but the $\chi_{\text{PID},K(\pi)}^2$ for kaon (pion) hypothesis is retained for further analysis in the signal-candidate selection.

Photon candidates from π^0 and Σ^0 decays are reconstructed from the electromagnetic showers detected in the EMC crystals. The deposited energy is required to be larger than 25 MeV in the barrel region with $|\cos\theta| < 0.80$ and larger than 50 MeV in the end-cap region with $0.86 < |\cos\theta| < 0.92$. To further suppress fake photon candidates due to electronic noise or beam-related background, the measured EMC time is required to be within 700 ns from the event start time. To reconstruct π^0 candidates, the invariant mass of a photon pair is required to satisfy $0.115 < M_{\gamma\gamma} < 0.150$ GeV/ c^2 . To further improve the momentum resolution, the invariant mass of the photon pair is constrained to the known π^0 mass [28] by applying a one-constraint kinematic fit, the χ^2 of which is required to be less than 200. The momentum of the π^0 after the fit is used in the subsequent analysis.

Neutral kaon candidates are reconstructed through the decay $K_S^0 \rightarrow \pi^+\pi^-$ by combining all pairs of oppositely charged tracks with both pions passing the PID requirement. These tracks, and also those used to build Λ candidates, must satisfy $|\cos\theta| < 0.93$ and $|V_z| < 20$ cm, while no V_r requirement is applied. A vertex fit is applied to pairs of charged tracks, constraining them to originate from a common decay vertex, and the χ^2 of this vertex fit is required to be less than 100. The invariant mass of the $\pi^+\pi^-$ pair needs to satisfy $0.487 < M_{\pi^+\pi^-} < 0.511$ GeV/ c^2 . Here, $M_{\pi^+\pi^-}$ is calculated with the pions constrained to originate at the decay vertex. To further suppress background, we require the ratio of the decay length to the resolution of decay length to be greater than 2. An analogous normalized decay-length requirement is imposed on Λ candidates reconstructed in the final state $p\pi^-$. Here a PID requirement is imposed on the proton candidate, but not on the π^- candidate. The invariant mass of the $p\pi^-$ combination must satisfy $1.111 < M_{p\pi^-} < 1.121$ GeV/ c^2 .

Protons and reconstructed π^0 mesons are used to form Σ^+ candidates. The invariant mass of the $p\pi^0$ pair is required to be $1.15 < M_{p\pi^0} < 1.28$ GeV/ c^2 , which is a

loose requirement since this kinematic variable is fitted to determine the Σ^+ signal.

When selecting $\Lambda_c^+ \rightarrow \Sigma^+\pi^+\pi^-$ decays we veto events where the invariant mass of the $\pi^+\pi^-$ pair satisfies $0.48 < M_{\pi^+\pi^-} < 0.52$ GeV/ c^2 , in order to avoid cross-contamination between $\Lambda_c^+ \rightarrow \Sigma^+K_S^0$ and $\Lambda_c^+ \rightarrow \Sigma^+\pi^+\pi^-$. Possible backgrounds from $\Lambda \rightarrow p\pi^-$ in the final states are also rejected by requiring $M(p\pi^-)$ lies outside the range (1.11, 1.12) GeV/ c^2 . Since the Λ background is not significant in $\Lambda_c^+ \rightarrow \Sigma^+K_S^0$ decays, a Λ veto is not imposed for the mode. If there are multiple Λ_c^+ combinations in a single event, we choose the candidate with the minimum magnitude of the energy difference, defined as $\Delta E \equiv E_{\Lambda_c} - E_{\text{beam}}$, where E_{Λ_c} is the energy of the detected Λ_c^+ candidate in the rest frame of the initial e^+e^- collision system, and E_{beam} is the beam energy. Furthermore, the requirement $-0.02 < \Delta E < 0.01$ GeV is imposed as illustrated in Fig. 1, where the cut values are decided from inspection of the figure-of-merit $\text{FOM} = \frac{S}{\sqrt{S+B}}$, where $S(B)$ is the number of signal (background) events in the inclusive MC samples.

The Σ^0 candidates are reconstructed from photon candidates and Λ candidates. To suppress backgrounds from energetic showers, we further require the deposited energies of the photon candidates to be less than 0.25 GeV in Σ^0 reconstruction. The invariant mass of the $\gamma\Lambda$ pair is required to lie within $1.179 < M_{\gamma\Lambda} < 1.203$ GeV/ c^2 .

When reconstructing the $\Lambda_c^+ \rightarrow \Sigma^0 K^+$ and $\Sigma^0 \pi^+$ signal decays, we perform a kinematic fit that constrains the invariant mass of the recoil side of the Λ_c^+ candidate to the known mass of the $\bar{\Lambda}_c^-$ [28]. To improve the resolution of photon momenta originating from Σ^0 , we also constrain the invariant masses of the $p\pi^-$ and $\gamma p\pi^-$ to the known masses of Λ and Σ^0 , respectively. The fitted momenta from this three-constraint (3C) kinematic fit are used in the subsequent analysis. The aforementioned ΔE metric can be used for selection the only candidate when there are multiple Λ_c^+ candidates in the event. But the $\chi_{\text{total}}^2 \equiv \chi_{3C}^2 + \chi_{\text{VF}}^2 + \chi_{\text{PID},h}^2$ metric gives better signal significance, where χ_{3C}^2 is the 3C fit quality and, χ_{VF}^2 is the quality of the vertex fit of the Λ reconstruction. The $\chi_{\text{PID},h}^2$ is defined as [45]

$$\chi_{\text{PID},h}^2 \equiv \left(\frac{t - t_h}{\sigma_{\text{TOF}}} \right)^2 + \left(\frac{dE/dx - (dE/dx)_h}{\sigma_{dE/dx}} \right)^2, \quad (1)$$

where t and dE/dx are the measured TOF and ionization energy loss, the index “ h ” denotes the values expected for the $h = \pi, K$ hypotheses and σ_{TOF} and $\sigma_{dE/dx}$ are the resolutions of TOF and dE/dx measurements, respectively. No explicit PID requirement is imposed on the particle that accompanies the Σ^0 , and the assignment of $\Lambda_c^+ \rightarrow \Sigma^0 K^+$ and $\Sigma^0 \pi^+$ modes is only based on χ_{total}^2 with the K and π hypotheses, respectively. To suppress backgrounds, a

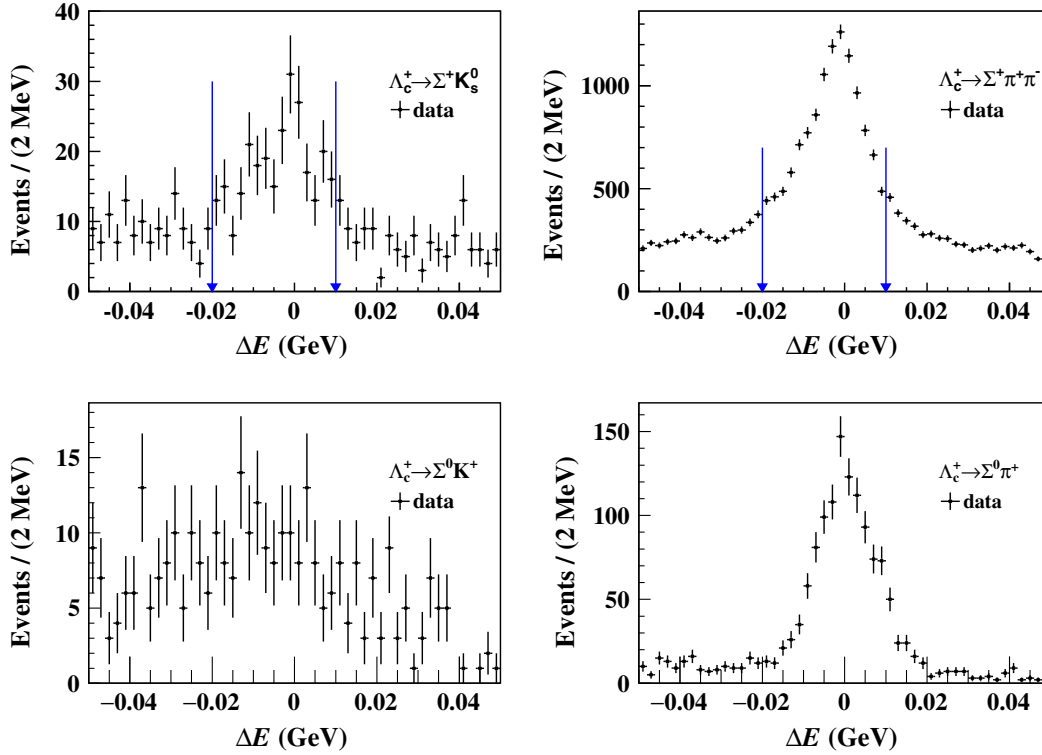


FIG. 1. ΔE distributions for the data samples passing the event selections. The arrows indicate the requirements for ΔE . For purpose of better illustration of the signal components, M_{BC} and $M_{p\pi^0}$ for $\Lambda_c^+ \rightarrow \Sigma^+ K_S^0$ and $\Sigma^+ \pi^+ \pi^-$ modes are further required to be within $\pm 3\sigma$ resolutions around individual peaks only here. The momenta before the kinematic fit are used for calculating ΔE of $\Lambda_c^+ \rightarrow \Sigma^0 K^+$ and $\Sigma^0 \pi^+$ modes.

requirement of $\chi_{\text{total}}^2 < 20$ is imposed for both modes, which gives best FOM values.

IV. RELATIVE BRANCHING FRACTION MEASUREMENTS

To determine the yields for the four signal Λ_c^+ decay modes, we use the beam-constrained mass M_{BC} , which is defined as

$$M_{\text{BC}} \equiv \sqrt{E_{\text{beam}}^2/c^4 - |\vec{p}_{\Lambda_c}|^2/c^2}, \quad (2)$$

where \vec{p}_{Λ_c} is the three-momentum of the tagged Λ_c^+ candidate in the rest frame of the initial e^+e^- collision system. To mitigate systematic uncertainties associate with the Σ detection, we measure the relative BFs of $R_{\Sigma^0 K^+} \equiv \mathcal{B}(\Lambda_c^+ \rightarrow \Sigma^0 K^+)/\mathcal{B}(\Lambda_c^+ \rightarrow \Sigma^0 \pi^+)$ and $R_{\Sigma^+ K_S^0} \equiv \mathcal{B}(\Lambda_c^+ \rightarrow \Sigma^+ K_S^0)/\mathcal{B}(\Lambda_c^+ \rightarrow \Sigma^+ \pi^+ \pi^-)$.

To determine $R_{\Sigma^0 K^+}$, the M_{BC} distributions of the $\Lambda_c^+ \rightarrow \Sigma^0 K^+$ and $\Sigma^0 \pi^+$ decays, as illustrated in Fig. 2, are fitted simultaneously for the seven energy points. In the unbinned extended maximum-likelihood fit, the signal shapes are derived from MC simulations convolved with Gaussian functions to account for the potential difference between

data the MC simulations, due to imperfect modeling in MC simulation and the beam-energy spread. The parameters of the Gaussian functions in the signal mode are the same as the reference mode, which are floating in the fit. The combinatorial background is described by an ARGUS function [46]

$$f^{\text{ARGUS}} \propto M_{\text{BC}} \sqrt{1 - \left(\frac{M_{\text{BC}} \cdot c^2}{E_{\text{beam}}}\right)^2} \times e^{a(1 - \frac{M_{\text{BC}} \cdot c^2}{E_{\text{beam}}})^2}, \quad (3)$$

where the parameter a is different in the signal and reference modes and the cut-off parameter is fixed to the beam energy E_{beam} at each energy point. The observed yield $n_{\Sigma^0 K^+}$ of $\Lambda_c^+ \rightarrow \Sigma^0 K^+$ decays is related to $n_{\Sigma^0 \pi^+}$, the yield of $\Lambda_c^+ \rightarrow \Sigma^0 \pi^+$ decays, by

$$n_{\Sigma^0 K^+} = R_{\Sigma^0 K^+} \cdot \frac{\varepsilon_{\Sigma^0 K^+}}{\varepsilon_{\Sigma^0 \pi^+}} \cdot n_{\Sigma^0 \pi^+}, \quad (4)$$

where $\varepsilon_{\Sigma^0 K^+}$ ($\varepsilon_{\Sigma^0 \pi^+}$) is the detection efficiency of $\Lambda_c^+ \rightarrow \Sigma^0 K^+$ ($\Lambda_c^+ \rightarrow \Sigma^0 \pi^+$) estimated with the signal MC samples. The relative BF $R_{\Sigma^0 K^+}$ is obtained directly in the simultaneous fit as summarized in Table II. The fit results are shown in Fig. 2.

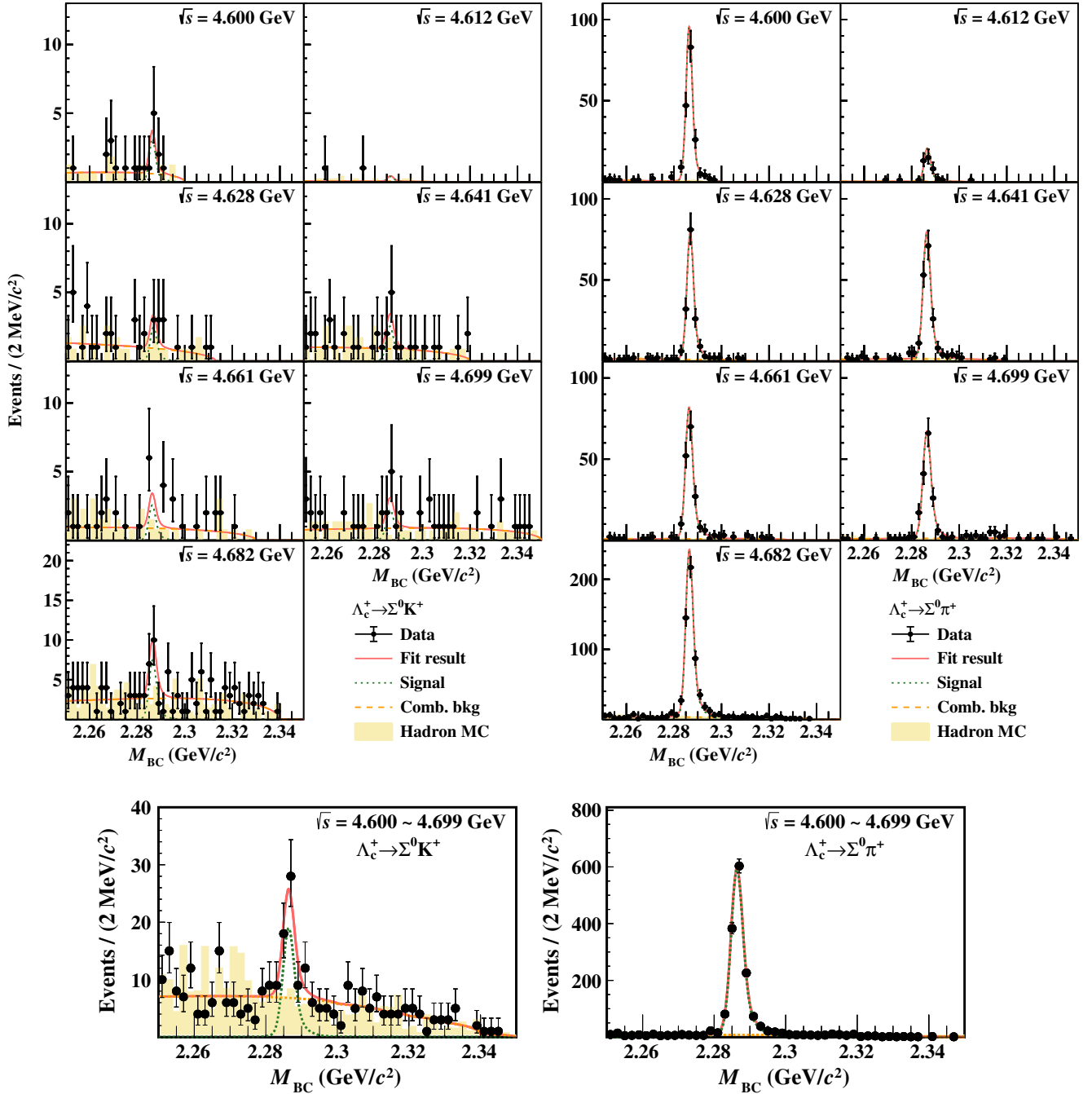


FIG. 2. The simultaneous fit results of the M_{BC} distributions for the $\Lambda_c^+ \rightarrow \Sigma^0 K^+$ and $\Sigma^0 \pi^+$ candidates at different energy points, where the black points with error bars denote data, the red solid lines denote the fit results, the green dotted lines denote the signal components and the orange dashed lines denote combinatorial backgrounds.

The decay $\Lambda_c^+ \rightarrow p K_S^0 \pi^0$ includes many resonant enhancements which may peak in the M_{BC} spectrum and potentially bias the measurement of $R_{\Sigma^+ K_S^0}$. A two-dimensional, i.e., M_{BC} and $M_{p\pi^0}$, unbinned fit is performed to distinguish the signal $\Lambda_c^+ \rightarrow \Sigma^+ K_S^0$ decay from other contributions.

In the simultaneous fit to the signal and the reference modes, we adopt two-dimensional signal shapes from MC

simulations convolved with two uncorrelated Gaussian functions to determine the yield $n_{\Sigma^+ K_S^0}$ for $\Lambda_c^+ \rightarrow \Sigma^+ K_S^0$ decays, which is related to $n_{\Sigma^+ \pi^+ \pi^-}$ by

$$n_{\Sigma^+ K_S^0} = R_{\Sigma^+ K_S^0} \cdot \frac{\mathcal{B}_{\text{inter}} \varepsilon_{\Sigma^+ K_S^0}}{\varepsilon_{\Sigma^+ \pi^+ \pi^-}} \cdot n_{\Sigma^+ \pi^+ \pi^-}, \quad (5)$$

where $\varepsilon_{\Sigma^+ K_S^0}$ ($\varepsilon_{\Sigma^+ \pi^+ \pi^-}$) is the detection efficiency of $\Lambda_c^+ \rightarrow \Sigma^+ K_S^0$ ($\Sigma^+ \pi^+ \pi^-$) estimated with signal MC samples, and

TABLE II. Integrated luminosities taken from Refs. [29,30], yields and detection efficiencies for the signal modes $\Lambda_c^+ \rightarrow \Sigma^0 K^+$ and $\Sigma^+ K_S^0$, as well as those for the reference modes $\Lambda_c^+ \rightarrow \Sigma^0 \pi^+$ and $\Sigma^+ \pi^+ \pi^-$ modes at the seven energy points. The uncertainties are statistical. Also listed are the results for the relative BF, where the first uncertainties are statistical, and the second are systematic.

| \sqrt{s} (GeV) | \mathcal{L}_{int} (pb $^{-1}$) | $n_{\Sigma^0 K^+}$ | $n_{\Sigma^0 \pi^+}$ | $10^2 \epsilon_{\Sigma^0 K^+}$ | $10^2 \epsilon_{\Sigma^0 \pi^+}$ | $n_{\Sigma^+ K_S^0}$ | $n_{\Sigma^+ \pi^+ \pi^-}$ | $10^2 \epsilon_{\Sigma^+ K_S^0}$ | $10^2 \epsilon_{\Sigma^+ \pi^+ \pi^-}$ |
|---|--|--------------------|----------------------|--------------------------------|----------------------------------|---|----------------------------|----------------------------------|--|
| 4.600 | 566.9 | 5.5 ± 1.2 | 178 ± 13 | 9.30 ± 0.04 | 10.79 ± 0.05 | 6.3 ± 1.9 | 900 ± 35 | 18.85 ± 0.06 | 19.92 ± 0.06 |
| 4.612 | 103.8 | 1.1 ± 0.3 | 38 ± 6 | 8.46 ± 0.04 | 10.02 ± 0.05 | 1.1 ± 0.3 | 157 ± 15 | 17.83 ± 0.06 | 19.26 ± 0.06 |
| 4.628 | 521.5 | 4.8 ± 1.0 | 156 ± 13 | 8.31 ± 0.04 | 9.71 ± 0.04 | 5.3 ± 1.6 | 778 ± 35 | 17.37 ± 0.06 | 18.83 ± 0.06 |
| 4.641 | 552.4 | 5.4 ± 1.2 | 174 ± 14 | 8.36 ± 0.04 | 9.76 ± 0.04 | 5.2 ± 1.6 | 783 ± 36 | 17.00 ± 0.06 | 18.65 ± 0.06 |
| 4.661 | 529.6 | 5.3 ± 1.1 | 173 ± 14 | 8.20 ± 0.04 | 9.60 ± 0.04 | 5.2 ± 1.6 | 770 ± 36 | 16.63 ± 0.06 | 18.18 ± 0.06 |
| 4.682 | 1669.3 | 16.4 ± 3.3 | 530 ± 24 | 8.22 ± 0.04 | 9.56 ± 0.04 | 15.9 ± 4.8 | 2395 ± 63 | 16.18 ± 0.06 | 17.92 ± 0.06 |
| 4.699 | 536.5 | 4.9 ± 1.1 | 159 ± 13 | 8.12 ± 0.04 | 9.47 ± 0.04 | 4.6 ± 1.4 | 694 ± 34 | 15.73 ± 0.06 | 17.62 ± 0.06 |
| $R_{\Sigma^0 K^+} = 0.0361 \pm 0.0073 \pm 0.0005$ | | | | | | $R_{\Sigma^+ K_S^0} = 0.0106 \pm 0.0031 \pm 0.0004$ | | | |

$\mathcal{B}_{\text{inter}} = \mathcal{B}(K_S^0 \rightarrow \pi^+ \pi^-)$ is taken from the PDG [28]. Three types of background components are included: (a) combinatorial backgrounds with no peaking structures in both dimensions, (b) non- Σ^+ background (mainly coming from nonsignal $\Lambda_c^+ \rightarrow p K_S^0 \pi^0$ decays), and (c) non- Λ_c^+ background from inclusive Σ^+ production. The combinatorial background component is described by a product of an ARGUS function in the M_{BC} dimension and a linear function in the $M_{p\pi^0}$ dimension

$$f^{\text{CombBkg}} \propto f^{\text{ARGUS}} \cdot [c_0 + c_1 M_{p\pi^0}], \quad (6)$$

where the parameter a of the f^{ARGUS} function is different from that in the fit of $\Lambda_c^+ \rightarrow \Sigma^0 K^+$ and $\Sigma^0 \pi^+$ decays, and c_0, c_1 are coefficients of the linear function. The approach for modeling the non- Σ^+ background is different between the signal and reference modes. For the reference mode, the shape of non- Σ^+ background is modeled with a product of the Λ_c^+ signal shape in M_{BC} and a linear function in $M_{p\pi^0}$. For the signal mode, the shape of the non- Σ^+ background coming from $\Lambda_c^+ \rightarrow p K_S^0 \pi^0$ decays is described by a two-dimensional shape derived from MC simulation in which intermediate states of the process $\Lambda_c^+ \rightarrow p K_S^0 \pi^0$ are considered. Other non- Σ^+ backgrounds from $\Lambda_c^+ \rightarrow p\eta, p\omega$, etc., are found to be negligible. The shape of non- Λ_c^+ backgrounds is described by a product of an ARGUS function in M_{BC} and the Σ^+ signal shape derived from MC simulations in $M_{p\pi^0}$. The yields of these background components are free parameters in the fit. When fitting $\Lambda_c^+ \rightarrow \Sigma^+ K_S^0$, an extra background component is included that accounts for non- K_S^0 contamination from the $\Lambda_c^+ \rightarrow \Sigma^+ \pi^+ \pi^-$ decays, whose shape is fixed according to MC simulations. The yield n_{cont} of this background is related to the fitted yield $n_{\Sigma^+ \pi^+ \pi^-}$ in the $\Lambda_c^+ \rightarrow \Sigma^+ \pi^+ \pi^-$ decay as follows:

$$n_{\text{cont}} = \frac{\epsilon_{\text{cont}}}{\epsilon_{\Sigma^+ \pi^+ \pi^-}} \cdot n_{\Sigma^+ \pi^+ \pi^-}. \quad (7)$$

Here ϵ_{cont} is the contamination rate of $\Lambda_c^+ \rightarrow \Sigma^+ \pi^+ \pi^-$ decays into the $\Lambda_c^+ \rightarrow \Sigma^+ K_S^0$ sample. The relative BF $R_{\Sigma^+ K_S^0}$ is obtained from the simultaneous fit of $\Lambda_c^+ \rightarrow \Sigma^+ K_S^0$ and $\Lambda_c^+ \rightarrow \Sigma^+ \pi^+ \pi^-$ decays, as summarized in Table II. The M_{BC} and $M_{p\pi^0}$ projections of the simultaneous two-dimensional fit of the signal and reference modes are shown in Figs. 3 and 4.

V. SYSTEMATIC UNCERTAINTIES

In the measurements of $R_{\Sigma^0 K^+}$ and $R_{\Sigma^+ K_S^0}$, the uncertainties associated with the Σ^0 and Σ^+ reconstruction cancel in the ratio. In the $R_{\Sigma^0 K^+}$ measurement, the equal number of charged tracks in the signal and reference modes means that any uncertainty in the tracking efficiency also cancels. Similarly, in the $R_{\Sigma^+ K_S^0}$ measurement, there is no uncertainty from PID as the same $\pi^+ \pi^-$ PID requirements are imposed in the K_S^0 reconstruction and for the reference mode $\Lambda_c^+ \rightarrow \Sigma^+ \pi^+ \pi^-$. Those uncertainties that do not cancel are summarized in Table III and discussed below.

- (I) *PID*. To account for the difference between data and MC simulation, we study a series of control samples of $e^+ e^- \rightarrow K^+ K^- \pi^+ \pi^-, K^+ K^- K^+ K^-, K^+ K^- \pi^+ \pi^- \pi^0, \pi^+ \pi^- \pi^+ \pi^-, \pi^+ \pi^- \pi^+ \pi^- \pi^0$ events [47] to determine the K^\pm and π^\pm PID efficiencies. The detection efficiencies for the four Λ_c^+ decay modes are recalculated after reweighting the corresponding MC samples on an event-by-event basis according to the momentum-dependent efficiency differences between data and MC simulations. The corrected efficiencies are then input to the simultaneous fits and the resultant changes are taken as the systematic uncertainty. The statistical fluctuations in the control samples also induce uncertainties in the reweighting procedure, which are evaluated in the different momentum regions and propagated to the final measurement. The average uncertainty is calculated as

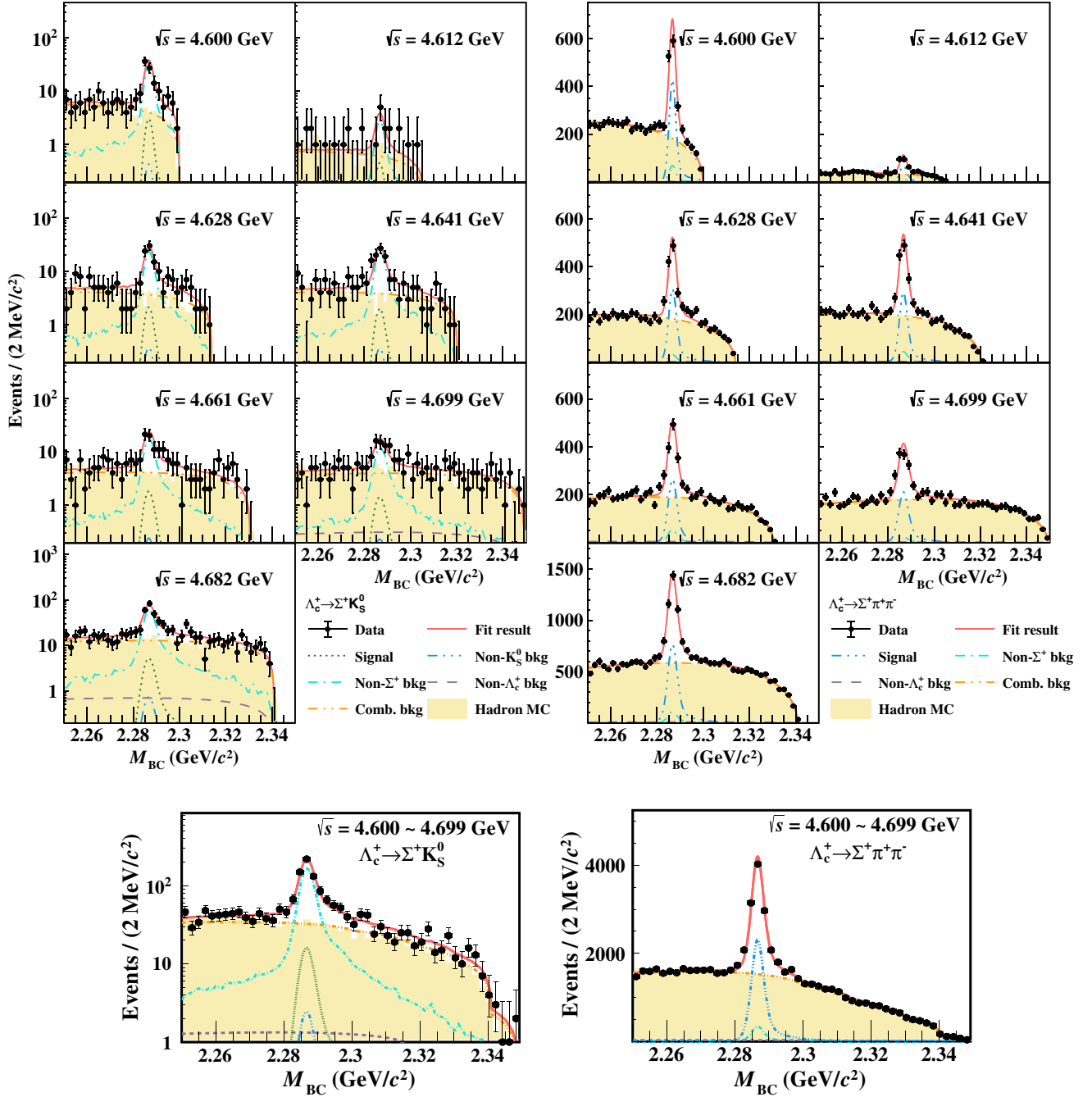


FIG. 3. The M_{BC} projections of the simultaneous two-dimensional fit of the $\Lambda_c^+ \rightarrow \Sigma^+ K_S^0$ and $\Sigma^+ \pi^+ \pi^-$ candidates at different energy points, where the black points with error bars denote data, the red solid lines denote the fit results, and the other colored curves denote the different components. In the left panel, the green dotted lines denote $\Lambda_c^+ \rightarrow \Sigma^+ K_S^0$ signal. In the right side, the blue dashed-dotted lines denote $\Lambda_c^+ \rightarrow \Sigma^+ \pi^+ \pi^-$ signal.

$$\sigma_{\text{sys.}} = \sqrt{\frac{1}{n_{\text{MC}}} \sum_{i=1}^{n_{\text{MC}}} \sigma_i^2}, \quad (8)$$

where n_{MC} is the size of the MC samples and σ_i is the statistical uncertainty of the control samples in the momentum region where the i th event in the MC

sample is found. We add these two contributions in quadrature to arrive at the total uncertainty from PID, which is 0.9% for $R_{\Sigma^0 K^+}$.

(II) *Tracking*. Using the same control samples to determine the π^\pm tracking efficiencies, we reweight the detection efficiency for $\Lambda_c^+ \rightarrow \Sigma^+ \pi^+ \pi^-$ and evaluate the systematic uncertainty in the same way as for the

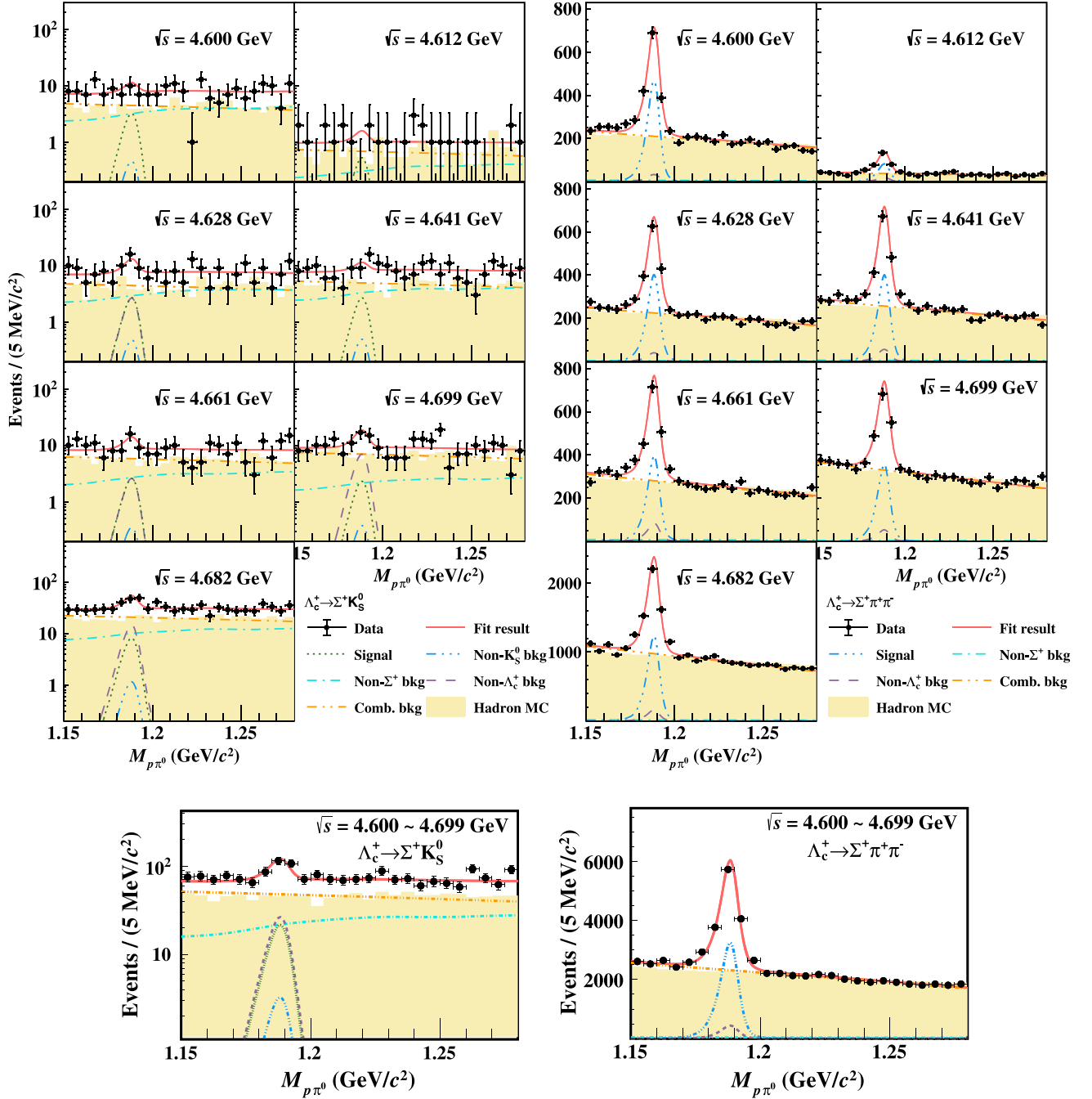


FIG. 4. The $M_{p\pi^0}$ projections of the simultaneous two-dimensional fit of the $\Lambda_c^+ \rightarrow \Sigma^+ K_S^0$ and $\Sigma^+ \pi^+ \pi^-$ candidates at different energy points, where the black points with error bars denote data, the red solid lines denote the fit results, and the other colored curves denote the different components. In the left panel, the green dotted lines denote $\Lambda_c^+ \rightarrow \Sigma^+ K_S^0$ signal. In the right side, the blue dashed-dotted lines denote $\Lambda_c^+ \rightarrow \Sigma^+ \pi^+ \pi^-$ signal.

PID, which results in a contribution of 1.0% for $R_{\Sigma^+ K_S^0}$.

- (III) K_S^0 reconstruction. The K_S^0 reconstruction efficiencies are studied by using control samples of $J/\psi \rightarrow K^*(892)^\pm K^\mp$, $K^*(892)^\pm \rightarrow K_S^0 \pi^\pm$ and $J/\psi \rightarrow \phi K_S^0 K^\mp \pi^\pm$ decays. The systematic uncertainty is

again evaluated in the same way as for the PID, which gives a contribution of 1.0% for $R_{\Sigma^+ K_S^0}$.

- (IV) $K_S^0(\Lambda)$ veto region. For the $\Lambda_c^+ \rightarrow \Sigma^+ \pi^+ \pi^-$ decay mode, the $K_S^0(\Lambda)$ veto may have a different efficiency in data and MC simulation. To bound any such bias, we remove the $K_S^0(\Lambda)$ veto and reevaluate

TABLE III. Summary of systematic uncertainties for relative BF measurements of the $\Lambda_c^+ \rightarrow \Sigma^0 K^+$ and $\Sigma^+ K_S^0$ decays. The total systematic uncertainty is the sum in quadrature of the individual components. “—” indicates cases where there is no uncertainty.

| Source | $R_{\Sigma^0 K^+}$ (%) | $R_{\Sigma^+ K_S^0}$ (%) |
|--|------------------------|--------------------------|
| PID | 0.9 | — |
| Tracking | — | 1.0 |
| K_S^0 reconstruction | — | 1.0 |
| K_S^0 veto region | — | 0.4 |
| Λ veto region | — | 0.4 |
| χ^2 requirement | 0.7 | — |
| ΔE requirement | — | 0.5 |
| Signal model | 0.5 | 2.5 |
| Fitting model | 0.6 | 1.6 |
| $\mathcal{B}(K_S^0 \rightarrow \pi^+ \pi^-)$ | — | 0.1 |
| Total | 1.4 | 3.4 |

the relative BFs. The relative difference between the reevaluated result and the nominal result is taken as the systematic uncertainty, which is 0.4%(0.4%) for $R_{\Sigma^+ K_S^0}$.

- (V) *Joint fit-quality χ^2_{total} requirement.* Joint fit-quality χ^2_{total} requirements are imposed on the $\Lambda_c^+ \rightarrow \Sigma^0 K^+$ and $\Sigma^0 \pi^+$ decay modes. To evaluate the effect of any difference between data and MC simulation, we fit to the χ^2_{total} distribution in data with the shapes derived from MC simulations convolved with a floating Gaussian function. The detection efficiency is re-measured after resampling the corresponding χ^2_{total} variable in MC samples according to the fitted Gaussian function, and $R_{\Sigma^0 K^+}$ is updated accordingly. The Gaussian parameters are randomly varied within the fitted uncertainties, and the corresponding value of $R_{\Sigma^0 K^+}$ is recorded. The mean μ_{χ^2} and the standard deviation σ_{χ^2} of the $R_{\Sigma^0 K^+}$ distribution is measured and $\sqrt{\mu_{\chi^2}^2 + \sigma_{\chi^2}^2}/R_{\Sigma^0 K^+}$ is assigned as the corresponding systematic uncertainty, which is 0.7%.
- (VI) *Energy difference ΔE requirement.* The energy difference ΔE requirement is used in the measurement of $R_{\Sigma^+ K_S^0}$. Following a similar procedure as for the χ^2 uncertainty, we first obtain the difference of ΔE distributions in data and MC simulations, and then study the distribution of the corresponding $R_{\Sigma^+ K_S^0}$ values with updated efficiencies, which leads to the assignment of a systematic uncertainty of 0.5% for $R_{\Sigma^+ K_S^0}$.
- (VII) *Signal model.* We use the phase-space model for simulating the $\Lambda_c^+ \rightarrow \Sigma^0 K^+$ and $\Lambda_c^+ \rightarrow \Sigma^+ K_S^0$ decay modes to obtain our central values, since the decay-asymmetry parameters are not known. As a system-

atic check, we test several extreme cases of the decay-asymmetry parameters and recalculate their detection efficiencies based on the corresponding signal MC samples. The resultant changes on the relative BFs are taken as the systematic uncertainties, which are 0.5% and 2.5% for $R_{\Sigma^0 K^+}$ and $R_{\Sigma^+ K_S^0}$, respectively.

- (VIII) *Fitting model.* The fitting procedure has uncertainties arising from both the signal and background shapes. For the signal shapes, the convolved Gaussian functions are varied by $\pm 1\sigma$ around their baseline values. For the $\Lambda_c^+ \rightarrow \Sigma^+ K_S^0$ mode, we also consider the effect of the correlation between the convolved Gaussian functions in M_{BC} and $M_{p\pi^0}$ by including a correlation coefficient determined from MC and verify that this leads to a negligible bias. For the background shapes, the parameter E_{beam} in the ARGUS function of Eq. (3) is randomly varied by ± 0.15 MeV and the shape of the $\Lambda_c^+ \rightarrow p K_S^0 \pi^0$ background component is replaced by a shape from an alternative partial wave analysis, in which more intermediate states are considered than those in the nominal signal MC simulation. To take into account these effects, 5000 pseudo datasets are sampled according to the bootstrap method [48]. For each pseudo dataset, the fitting models are varied randomly. Pull distributions are inspected from these pseudo datasets, and the small biases of 0.6% and 1.6% are assigned as the systematic uncertainties for $R_{\Sigma^0 K^+}$ and $R_{\Sigma^+ K_S^0}$, respectively.
- (IX) $\mathcal{B}(K_S^0 \rightarrow \pi^+ \pi^-)$. The uncertainty on the BF $\mathcal{B}(K_S^0 \rightarrow \pi^+ \pi^-)$ [28] is propagated to give a systematic uncertainty of 0.1% in $R_{\Sigma^+ K_S^0}$.

VI. SUMMARY

In summary, based on 4.5 fb⁻¹ of e^+e^- annihilation data collected in the energy region between 4.6 GeV and 4.7 GeV with the BESIII detector at BEPCII, we report the measurements of BFs of the two singly Cabibbo-suppressed decay modes $\Lambda_c^+ \rightarrow \Sigma^0 K^+$ and $\Sigma^+ K_S^0$ relative to the reference modes $\Lambda_c^+ \rightarrow \Sigma^0 \pi^+$ and $\Sigma^+ \pi^+ \pi^-$, respectively. The BF of $\Lambda_c^+ \rightarrow \Sigma^0 K^+$ relative to $\Lambda_c^+ \rightarrow \Sigma^0 \pi^+$ is measured to be $0.0361 \pm 0.0073(\text{stat.}) \pm 0.0005(\text{syst.})$, while the BF of $\Lambda_c^+ \rightarrow \Sigma^+ K_S^0$ relative to $\Lambda_c^+ \rightarrow \Sigma^+ \pi^+ \pi^-$ is measured to be $0.0106 \pm 0.0031(\text{stat.}) \pm 0.0004(\text{syst.})$. Taking the world-average BFs $\mathcal{B}(\Lambda_c^+ \rightarrow \Sigma^0 \pi^+) = (1.29 \pm 0.07)\%$ and $\mathcal{B}(\Lambda_c^+ \rightarrow \Sigma^+ \pi^+ \pi^-) = (4.50 \pm 0.25)\%$ from the PDG [28], yields the absolute BF $\mathcal{B}(\Lambda_c^+ \rightarrow \Sigma^0 K^+) = (4.7 \pm 0.9(\text{stat.}) \pm 0.1(\text{syst.}) \pm 0.3(\text{ref.})) \times 10^{-4}$, and $\mathcal{B}(\Lambda_c^+ \rightarrow \Sigma^+ K_S^0) = (4.8 \pm 1.4(\text{stat.}) \pm 0.2(\text{syst.}) \pm 0.3(\text{ref.})) \times 10^{-4}$. This is the first measurement of the $\Lambda_c^+ \rightarrow \Sigma^+ K_S^0$ branching fraction. The $\Lambda_c^+ \rightarrow \Sigma^0 K^+$ BF is measured with a comparable precision to the combined

result from the Belle [9] and BABAR [10] collaborations. The ratio $\mathcal{B}(\Lambda_c^+ \rightarrow \Sigma^0 K^+)/\mathcal{B}(\Lambda_c^+ \rightarrow \Sigma^+ K_S^0)$ is determined to be $0.98 \pm 0.35(\text{stat.}) \pm 0.04(\text{syst.}) \pm 0.08(\text{ref.})$, which is consistent with the predictions in Refs. [3,5] under $SU(3)_F$ flavor symmetry and disfavors the prediction in Ref. [6]. The prediction for $\mathcal{B}(\Lambda_c^+ \rightarrow \Sigma^+ K_S^0)$ in Ref. [6] differs from our result by 2.5σ , indicating a reassessment of the IRA method may be needed. Though our work is generally consistent with the predictions in Refs. [2–5] within $1 \sim 2\sigma$, these theoretical predictions generally overestimate the BFs. The systematic uncertainties of our results are smaller than those of from the Belle and BABAR collaborations, but our precision is limited by the relatively low sample size. With the additional data which are foreseen to be collected near the $\Lambda_c^+ \bar{\Lambda}_c^-$ threshold in the coming years [49], we expect our measurements to improve in precision, and shed more light on the topic of charmed baryon decays.

ACKNOWLEDGMENTS

The BESIII collaboration thanks the staff of BEPCII and the IHEP computing center for their strong support. This work is supported in part by National Key R&D Program of China under Contracts No. 2020YFA0406400, No. 2020YFA0406300; National Natural Science Foundation of China (NSFC) under Contracts No. 11635010, No. 11675275, No. 11735014, No. 11822506, No. 11835012, No. 11935015, No. 11935016, No. 11935018, No. 11961141012, No. 12022510, No. 12025502, No. 12035009, No. 12035013, No. 12175321, No. 12192260,

No. 12192261, No. 12192262, No. 12192263, No. 12192264, No. 12192265; the Chinese Academy of Sciences (CAS) Large-Scale Scientific Facility Program; Joint Large-Scale Scientific Facility Funds of the NSFC and CAS under Contract No. U1832207, No. U1932101; State Key Laboratory of Nuclear Physics and Technology, PKU under Grant No. NPT2020KFY04; CAS Key Research Program of Frontier Sciences under Contract No. QYZDJ-SSW-SLH040; 100 Talents Program of CAS; the Fundamental Research Funds for the Central Universities; INPAC and Shanghai Key Laboratory for Particle Physics and Cosmology; ERC under Contract No. 758462; European Union’s Horizon 2020 research and innovation programme under Marie Skłodowska-Curie grant agreement under Contract No. 894790; German Research Foundation DFG under Contracts Nos. 443159800, Collaborative Research Center CRC 1044, GRK 2149; Istituto Nazionale di Fisica Nucleare, Italy; Ministry of Development of Turkey under Contract No. DPT2006K-120470; National Science and Technology fund; National Science Research and Innovation Fund (NSRF) via the Program Management Unit for Human Resources & Institutional Development, Research and Innovation under Contract No. B16F640076; STFC (United Kingdom); Suranaree University of Technology (SUT), Thailand Science Research and Innovation (TSRI), and National Science Research and Innovation Fund (NSRF) under Contract No. 160355; The Royal Society, UK under Contracts No. DH140054, No. DH160214; The Swedish Research Council; U.S. Department of Energy under Contract No. DE-FG02-05ER41374.

-
- [1] G. Abrams *et al.*, *Phys. Rev. Lett.* **44**, 10 (1980).
 - [2] T. Uppal, R. C. Verma, and M. P. Khanna, *Phys. Rev. D* **49**, 3417 (1994).
 - [3] J. Zou, F. Xu, G. Meng, and H. Y. Cheng, *Phys. Rev. D* **101**, 014011 (2020).
 - [4] H. J. Zhao, Y. L. Wang, Y. K. Hsiao, and Y. Yu, *J. High Energy Phys.* **02** (2020) 165.
 - [5] C. Geng, C. W. Liu, and T. H. Tsai, *Phys. Lett. B* **794**, 19 (2019).
 - [6] F. Huang, Z. P. Xing, and X. G. He, *J. High Energy Phys.* **03** (2022) 143.
 - [7] H. Y. Cheng, *Chin. J. Phys. (Taipei)* **78**, 324 (2022).
 - [8] W. M. Yao *et al.* (Particle Data Group), *J. Phys. G* **33**, 1 (2006).
 - [9] K. Abe *et al.* (Belle Collaboration), *Phys. Lett. B* **524**, 33 (2002).
 - [10] B. Aubert *et al.* (BABAR Collaboration), *Phys. Rev. D* **75**, 052002 (2007).
 - [11] H. Y. Cheng, X. W. Kang, and F. Xu, *Phys. Rev. D* **97**, 074028 (2018).
 - [12] H. N. Li, C. D. Lu, and F. S. Yu, *Phys. Rev. D* **86**, 036012 (2012).
 - [13] M. Saur and F. S. Yu, *Sci. Bull.* **65**, 1428 (2020).
 - [14] S. Bianco, F. L. Fabbri, D. Benson, and I. Bigi, *Riv. Nuovo Cimento* **26**, 1 (2003).
 - [15] M. Ablikim *et al.* (BESIII Collaboration), *Phys. Rev. Lett.* **116**, 052001 (2016).
 - [16] H. B. Li and X. R. Lyu, *Natl. Sci. Rev.* **8**, nwab181 (2021).
 - [17] R. Aaij *et al.* (LHCb Collaboration), *Phys. Rev. Lett.* **121**, 092003 (2018).
 - [18] R. Aaij *et al.* (LHCb Collaboration), *Phys. Rev. D* **100**, 032001 (2019).
 - [19] R. Aaij *et al.* (LHCb Collaboration), *Sci. Bull.* **67**, 479 (2022).
 - [20] H. Y. Cheng, *Sci. Bull.* **67**, 445 (2022).

- [21] F. Abudinén *et al.* (Belle II Collaboration), [arXiv:2206.15227](#).
- [22] M. Ablikim *et al.* (BESIII Collaboration), *Phys. Rev. Lett.* **115**, 221805 (2015).
- [23] M. Ablikim *et al.* (BESIII Collaboration), *Phys. Lett. B* **767**, 42 (2017).
- [24] M. Ablikim *et al.* (BESIII Collaboration), *Phys. Rev. Lett.* **121**, 251801 (2018).
- [25] Y. B. Li *et al.* (Belle Collaboration), *Phys. Rev. Lett.* **127**, 121803 (2021).
- [26] Y. B. Li *et al.* (Belle Collaboration), *Phys. Rev. D* **105**, L091101 (2022).
- [27] A. Chodos, R. L. Jaffe, K. Johnson, and C. B. Thorn, *Phys. Rev. D* **10**, 2599 (1974).
- [28] P. Zyla *et al.* (Particle Data Group), *Prog. Theor. Exp. Phys.* **2020**, 083C01 (2020).
- [29] M. Ablikim *et al.* (BESIII Collaboration), *Chin. Phys. C* **39**, 093001 (2015).
- [30] M. Ablikim *et al.* (BESIII Collaboration), [arXiv:2205.04809](#).
- [31] M. Ablikim *et al.* (BESIII Collaboration), *Nucl. Instrum. Methods Phys. Res., Sect. A* **614**, 345 (2010).
- [32] C. H. Yu *et al.*, in *Proceedings of IPAC2016, Busan, Korea* (JACoW, Geneva, Switzerland, 2016), 10.18429/JACoW-IPAC2016-TUYA01.
- [33] X. Li *et al.*, *Radiat. Detect. Technol. Methods* **1**, 13 (2017); Y. X. Guo *et al.*, *Radiat. Detect. Technol. Methods* **1**, 15 (2017); P. Cao *et al.*, *Nucl. Instrum. Methods Phys. Res., Sect. A* **953**, 163053 (2020).
- [34] S. Agostinelli *et al.*, *Nucl. Instrum. Methods Phys. Res., Sect. A* **506**, 250 (2003).
- [35] Z. Y. You, Y. T. Liang, and Y. J. Mao, *Chin. J. Phys.* **32**, 572 (2008).
- [36] Y. T. Liang *et al.*, *Nucl. Instrum. Methods Phys. Res., Sect. A* **603**, 325 (2009).
- [37] S. Jadach, B. F. L. Ward, and Z. Was, *Phys. Rev. D* **63**, 113009 (2001).
- [38] E. Richter-Was, *Phys. Lett. B* **303**, 163 (1993).
- [39] S. Jadach, B. F. L. Ward, and Z. Was, *Comput. Phys. Commun.* **130**, 260 (2000).
- [40] D. J. Lange, *Nucl. Instrum. Methods Phys. Res., Sect. A* **462**, 152 (2001).
- [41] R. G. Ping, *Chin. Phys. C* **32**, 599 (2008).
- [42] J. C. Chen, G. S. Huang, X. R. Qi, D. H. Zhang, and Y. S. Zhu, *Phys. Rev. D* **62**, 034003 (2000).
- [43] R. L. Yang, R. G. Ping, and H. Chen, *Chin. Phys. Lett.* **31**, 061301 (2014).
- [44] H. Chen and R. G. Ping, *Phys. Rev. D* **99**, 114027 (2019).
- [45] D. M. Asner *et al.*, *Int. J. Mod. Phys. A* **24**, 23 (2009).
- [46] H. Albrecht *et al.* (ARGUS Collaboration), *Phys. Lett. B* **241**, 278 (1990).
- [47] M. Ablikim *et al.* (BESIII Collaboration), *Phys. Rev. D* **99**, 112005 (2019).
- [48] M. R. Chernick, *Bootstrap Methods: A Guide for Practitioners and Researchers* (John Wiley & Sons, New York, 2011), Vol. 619.
- [49] M. Ablikim *et al.* (BESIII Collaboration), *Chin. Phys. C* **44**, 040001 (2020).